Materials Advances

ROYAL SOCIETY OF CHEMISTRY

PAPER

View Article Online
View Journal | View Issue

Cite this: *Mater. Adv.*, 2025, 6, 3841

Temperature-responsive fluorescent polygalacturonic acid: a step towards wound monitoring with smartphone imaging†

Dana Kaafarani, Jad Kaj and Pierre Karam *

Received 17th March 2025,
Accepted 26th April 2025

DOI: 10.1039/d5ma00236b

rsc.li/materials-advances

An increase in the temperature at the wound site is an early indication of a disturbance in the healing process and a sign of an infection. Different polymeric materials have been employed in wound dressing, including polygalacturonic acid (PGA). In this study, we complexed PGA to poly(phenylene ethynylene) (PPE-CO_2-108) to develop a fluorescence-based thermal sensor for solution and dry polymer film applications. The thermal sensor sensitivity and reversibility were tuned by changing the concentration of PGA and the solution ionic strength. As a result, we were able to create a highly reversible thermal sensor and by simply altering the ionic strength, we developed a sensor with long-lasting temperature memory. In solution, the macromolecule complexes had an absolute sensitivity of 0.013 $°C^{-1}$ (20–40 °C) and 0.029 $°C^{-1}$ (45–90 °C) when prepared in 150 mM NaCl. In the absence of NaCl, the sensor had a wider range, and its absolute sensitivity increased to 0.044 $°C^{-1}$ (20–90 °C). The sensor was also prepared into dried thin materials to mimic a wound suture with good thermal sensitivity over physiologically relevant temperatures. The calculated absolute sensitivity was equal to 0.011 $°C^{-1}$ between 25 and 55 °C. Using a home-developed app, we were able to accurately measure the temperature of these films. As such, our formulated PGA materials have the potential to be developed into smart sutures to monitor early signs of wound infection.

Introduction

Wounds provide an ideal environment for microorganisms to thrive.[1,2] After any surgical procedure or injury, the healing process starts and consists of different overlapping stages of reaction, regeneration, and remodeling, involving interactions between different types of cells.[3–8] The inflammatory response is part of the healing process and is characterized by the response of immune cells to tissue damage.[3,9] However, different factors, including pathogens, can disturb the healing of the wound, causing infection,[3] which delays the healing process.[10] For example, The wound healing process is associated with changes in pH values; a drop toward neutral to acidic pH indicates that the wound is recovering.[11,12] Consequently, bacterial metabolism triggers inflammation and induces an immune response characterized by increased blood flow to the affected area. This immune response results in temperature increase on the wound site.

Given the complexity of the process, many sensors have been developed to monitor the progress of wound healing.[13–18] Several studies have reported that a temperature increase greater than 3 °C around the wound most likely indicates signs of infection.[19] Therefore, it is important to provide efficient tools to accurately detect any possible infection for early treatment before it becomes severe.[20] This could be made possible by developing smart sutures with thermal sensing capabilities.

Our laboratory has exploited the unique photophysical properties of conjugated polyelectrolytes (CPEs) when complexed to polyvinylpyrrolidone, polyvinylpyrrolidone/vinyl acetate, poly(diallyldimethylammonium chloride), and polyvinylpyrrolidone-*co*-polystyrene to develop sensitive thermal sensors for the detection of temperature fluctuations in solution, hydrogel, thin films, and lipid membranes.[21–27] Specifically, PPE-CO_2, given its highly hydrophobic backbone, tends to aggregate in solution leading to a broad emission with a maximum peak at 520 nm.[28,29] In contrast, when dissolved in a non-polar solvent, the individual/disaggregated chain emission is well structured with a max emission at 450 nm.[28,29] This big shift in the fluorescent emission provides a tool to accurately probe thermally induced changes in the conjugated polyelectrolyte microenvironment.

Polygalacturonic acid (PGA) is a natural polysaccharide, used in wound dressings and anti-adhesive applications.[5,30] Tests on PGA showed that it exhibits important bio-adhesive properties and is better than other acidic polysaccharides.[31]

Department of Chemistry, American University of Beirut, P.O. Box 11-0236, Beirut, Lebanon. E-mail: pierre.karam@aub.edu.lb; Fax: +961-1-350000 Ext. 3970; Tel: +961-1-350000 Ext. 3989

† Electronic supplementary information (ESI) available:Additional fluorescence spectroscopy measurements. See DOI: https://doi.org/10.1039/d5ma00236b

Its backbone presents a great opportunity to tune the photophysical properties of the stiff PPE-CO_2-108 to develop a temperature sensor that could potentially address the aforementioned objective.

In this study, we report on the development of a fluorescence-based thermal sensor using PGA and PPE-CO_2-108. Both of these polymers are biocompatible and have shown little cytotoxicity against human cells.[32–35] We showed that by tuning the concentration of PGA and NaCl, we were able to develop fluorescent thermal sensors with tunable reversibility and sensitivity in solution. Dried films of the PGA-based thermal sensor were also prepared and tested at different temperatures. The change in fluorescent sensing was measured using an in-house developed app, which allowed us to convert recorded images from a smartphone into temperature readings.

Results and discussion

Photophysical properties of PGA/PPE-CO_2-108

The fluorescent behavior of conjugated polyelectrolytes is highly influenced by their microenvironment,[36] especially when mixed with other large macromolecules. In what follows, we detail our attempt to tune and manipulate this temperature/ionic strength dependency to prepare thermal sensors with high sensitivity and tunable reversibility using PGA.

Pristine PPE-CO_2-108, when heated in solution, showed a reversible increase in the fluorescent intensity at 450 nm (Fig. S1, ESI†). This observation is the result of the thermally induced shift towards the disaggregated conjugated polyelectrolyte which becomes the dominant species at higher temperatures and whose maximum emission is at 450 nm. The fluorescent enhancement also increased with the ionic strength; the maximum recorded intensity at 90 °C increased from 1.3 to 2.0 and then to 3.4 as the Na^+ concentration increased from 0 to 150 mM and then to 300 mM, respectively. This fundamental correlation between the structural changes of the conjugate polyelectrolytes and their photophysics and the effect of NaCl is what guided us while developing the thermal sensor in complexation with PGA.

To study the effect of PGA on the PPE-CO_2-108, the absorbance spectra of the CPE were measured before and after adding PGA in HEPES buffer (10 mM, pH = 7.0, 150 mM NaCl) Fig. 1C. Upon addition of 1.7 mg mL^{-1} PGA, a 6 nm red-shift to 439 nm was observed. The observed shift indicates stronger π–π interactions between the polyelectrolyte chains, resulting in increased conjugation length and planarization in the polyelectrolyte.[36,37] This extension in conjugation leads to a shift in the electronic and vibronic energy levels to lower energy.[38] A red-shift in the absorption band of poly(phenylene ethynylene) was previously reported and was associated with an increase in chain length, and complexing the

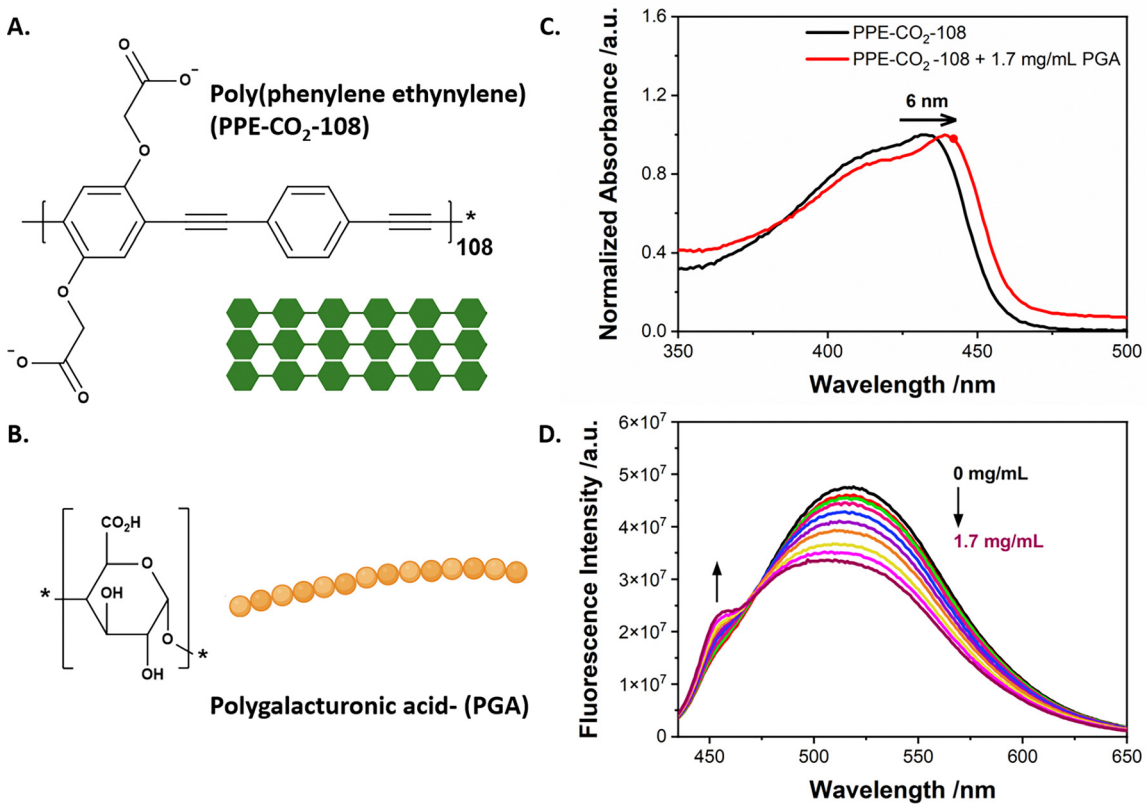

Fig. 1 Chemical structures of (A) poly(phenylene ethynylene) carboxylate with an average of 108 repeating units (PPE-CO_2-108) and (B) polygalacturonic acid (PGA) along with their cartoon representation. (C) Absorbance spectra of PPE-CO_2-108 before and after adding 1.7 mg mL^{-1} PGA. (D) Emission spectra of PPE-CO_2-108 upon incremental addition of PGA. Measurements in (C) and (D) were done in HEPES buffer (10 mM, pH = 7.0) and NaCl (150 mM). The samples in (D) were excited at 405 nm.

polyelectrolyte with different amphiphilic polymers and cationic polyelectrolytes.[29,39,40]

Next, we measured the emission spectra of PPE-CO_2-108 upon incremental addition of PGA in HEPES buffer (10 mM, pH = 7.0, 150 mM NaCl). As shown in Fig. 1D, the emission spectrum of pristine PPE-CO_2-108 exhibited a broad, structureless peak centered at 520 nm as the result of the aggregated CPEs which are believed to emit from an excimer-like state.[29] With the addition of PGA, we observed a decrease in the fluorescence intensity at 520 nm accompanied by the emergence of a new peak at 450 nm reflecting the disaggregation of the CPE polymer chains.[41,42] This disaggregation is mostly driven by hydrogen bonding-based interactions between the electronegative oxygen on the polyelectrolyte and the hydrogen atoms of the hydroxyl group of the polysaccharide. As the concentration of PGA increased, more hydrogen bonding interactions were made possible, which drove the disaggregation of PPE-CO_2-108 and resulted in further enhancement in the peak at 450 nm. The disaggregation was not as efficient as when PVP-based polymers were used but was enough to slightly destabilize the aggregates to induce thermal actuation.[21,43]

Thermal modulation of fluorescence in PGA/PPE-CO_2-108

Based on the titration experiment (Fig. 1D) and the thermal response reversibility of pristine PPE-CO_2-108 (Fig. S1, ESI†), we selected two concentrations of PGA to test their thermal response: the first concentration was chosen at the point where the PPE-CO_2-108 is starting to disaggregate and the 450 nm peak is barely visible (0.35 mg mL^{-1}). The second chosen concentration was at 1.7 mg mL^{-1} which shows a visible peak at 450 nm, an indication of the disaggregated CPEs. These selected concentrations were tested in the absence of NaCl and the presence of 150 mM NaCl since at low ionic strength, the negatively charged side chains would destabilize the PPE-CO_2-108 aggregates and allow for better interactions with the PGA polymer (Fig. S2, ESI†).[44] The thermal sensing properties of our mixtures were then studied by acquiring emission spectra with the increase in temperature, from 20 °C to 90 °C, with 5 °C increments. After each increase in temperature, the solution was kept for 2 minutes to stabilize and for the temperature to homogenize. At both PGA concentrations, mainly a broad 520 nm emission peak was observed at 20 °C. As we increased the temperature of the solution, the fluorescent intensity at 520 nm gradually decreased, while that at 450 nm emerged, attributed to the emission of disaggregated PPE-CO_2 chains. The thermal sensitivity was calculated as the ratio of the maximum intensity at 450 nm to that at 520 nm and plotted against the measured temperature. The thermal response of PGA/PPE-CO_2-108 was divided over two windows: the first one between 20 and 40 °C and the second between 45 and 90 °C. The relative sensitivity (S_r) was calculated using the following

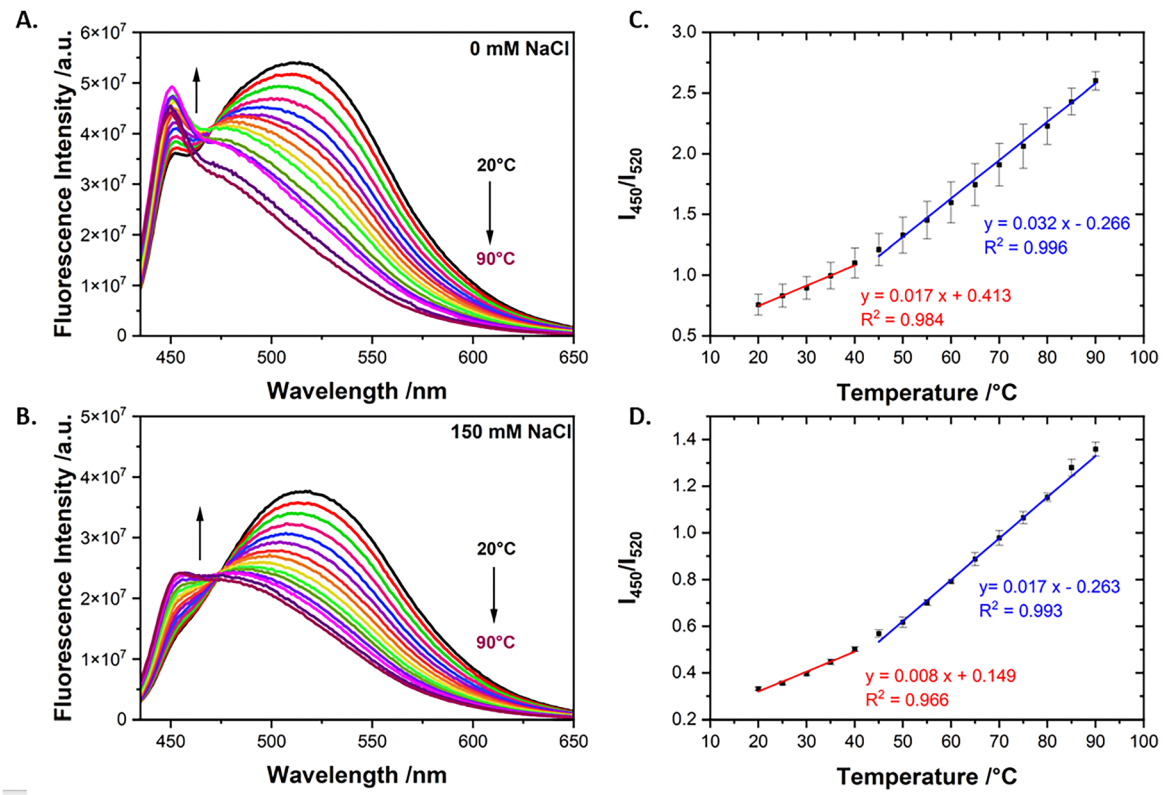

Fig. 2 (A) Fluorescent thermal response of PPE-CO_2-108 with 0.35 mg mL^{-1} PGA upon an increase in temperature of the solution from 20 °C to 90 °C with 5 °C increments in 0 mM NaCl and (B) 150 mM NaCl. (C) and (D) Ratiometric fluorescent thermal response was calculated from the ratio of 450 and 520 nm from (A) and (B), respectively. The red and blue lines represent the linear regression fit, based on three runs. Measurements were done in HEPES buffer (10 mM, pH = 7.0) with 0 mM NaCl and (D) 150 mM NaCl. The samples were excited at 405 nm.

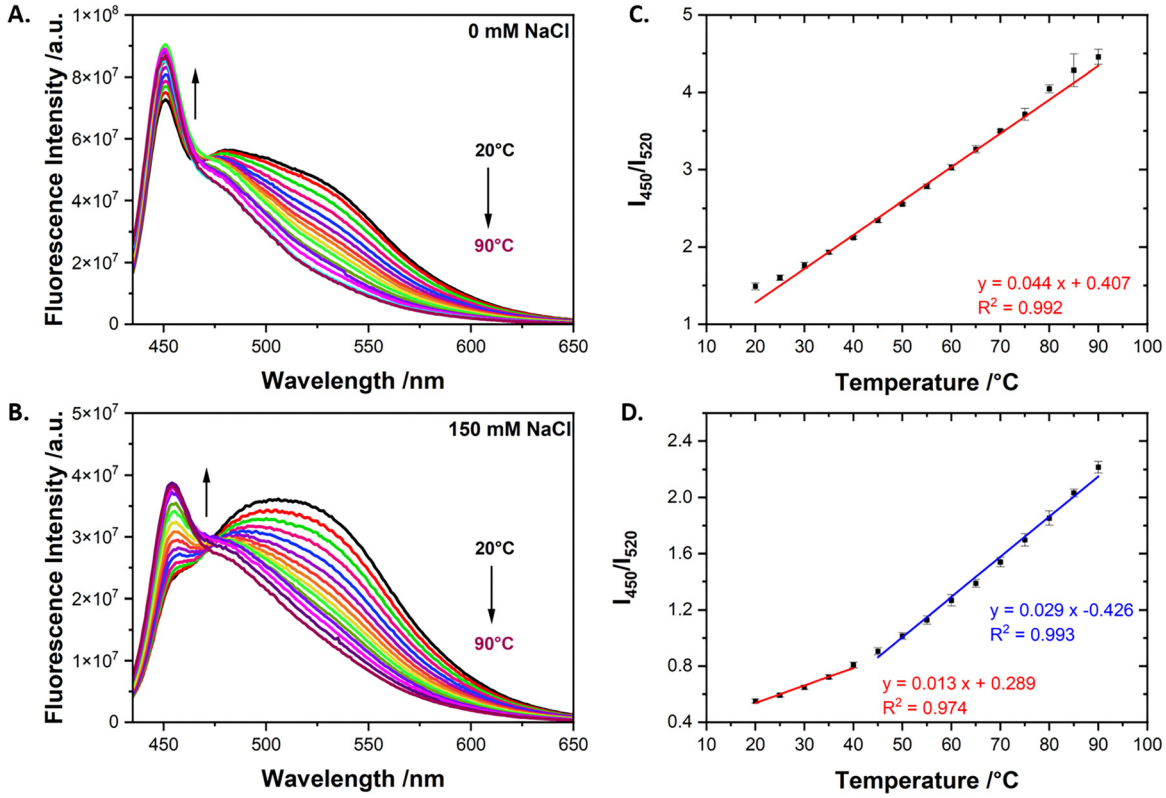

Fig. 3 (A) Fluorescent thermal response of PPE-CO_2-108 with 1.7 mg mL^{-1} PGA upon an increase in temperature of the solution from 20 °C to 90 °C with 5 °C increments in 0 mM NaCl and (B) 150 mM NaCl. (C) and (D) Ratiometric fluorescent thermal response was calculated from the ratio of 450 and 520 nm from (A) and (B), respectively. The red and blue lines in (C) and (D) represent the linear regression fit, based on three runs. Measurements were all done in HEPES buffer (10 mM, pH = 7.0) The samples were excited at 405 nm.

equation:

$$S_r = \frac{1}{Q_T}\frac{\Delta Q}{\Delta T} \times 100$$

where Q_T is I_{450}/I_{520} and $\Delta Q/\Delta T$ is the absolute sensitivity.

At low PGA concentration (0.35 mg mL^{-1}), the calculated absolute sensitivity was 0.008 $°C^{-1}$ and 0.017 $°C^{-1}$ at 20–40 °C and 45–90 °C, respectively, in 150 mM NaCl (Fig. 2D). The calculated absolute sensitivities in the absence of NaCl were higher at 0.017 $°C^{-1}$ and 0.032 $°C^{-1}$ (Fig. 2C). The sensors exhibited a maximum relative sensitivity of 2.99 $°C^{-1}$ at 45 °C when measured in the presence of 150 mM NaCl, and 2.65%$°C^{-1}$ at 45 °C in 0 mM NaCl.

At higher PGA concentration (1.7 mg mL^{-1}), in addition to the structureless peak centered at 520 nm, a more pronounced peak at 450 nm was initially observed, especially in the absence of NaCl (Fig. 3A). The ratiometric response for the solution prepared in 150 mM NaCl over the two regions resulted in absolute sensitivities of 0.013 $°C^{-1}$ and 0.029 $°C^{-1}$ and a maximum relative sensitivity of 3.21% $°C^{-1}$ at 45 °C (Fig. 3D). In the absence of NaCl, the thermal response was linear across the entire tested thermal window with an absolute sensitivity of 0.044 $°C^{-1}$ and a maximum relative sensitivity of 2.95% $°C^{-1}$ at 20 °C (Fig. 3C). The higher thermal sensitivity with increased PGA concentrations and lower ionic strengths is believed to be driven by the enhanced stabilization effect (Table S1, ESI†). In the absence of NaCl, some of the PPE-CO_2-108 chains are already destabilized at 20 °C, as signified by the small but apparent peak at 450 nm, so the added thermal energy is mostly acting on further disaggregating the CPE chains to be subsequently stabilized by PGA. At higher ionic strengths, however, we hypothesize that some of the added thermal energy is being directed toward destabilizing the CPE aggregates. As such, higher thermal sensitivity is observed at the lower ionic strength. For instance, when the sensitivity was monitored in a solution at even higher ionic strength (300 mM NaCl), it was lower than that measured at 150 mM NaCl and did not change substantially with the increase of PGA concentrations (Table S1, ESI†). In addition, when incremental amounts of PGA were added to a PPE-CO_2 solution in the absence of NaCl, a substantial increase in the fluorescence intensity at 450 nm was observed as compared to Fig. 1D measured in the presence of NaCl (Fig. S2, ESI†). Our hypothesis was also verified by lifetime data, reported later in the discussion. This is explained by the macromolecular level interactions established so far; if the PPE-CO_2-108 chains are already stabilized, here by the Na^+ counter ions, the thermal sensitivity and dynamic range would have been compromised.

The absolute sensitivity of the best-performing PGA/PPE-CO_2-108 mixture exceeded any of our previously reported conjugated polyelectrolyte-thermal sensors. The ratiometric thermal sensors based on PPE-CO_2 complexed with poly-vinylpyrrolidone (PVP)[43] and poly(diallyldimethylammonium chloride) (PDDA)[39]

Table 1 Time-resolved lifetime measurements for PGA/PPE-CO_2-108 under different experimental conditions

Sample	Ampl.	τ_1 (ns)	Ampl.	τ_2 (ns)
PGA/PPE-CO_2-108 + HEPES	0.37	0.493	0.58	3.68
PGA/PPE-CO_2-108 + HEPES (Heated)	0.44	0.426	0.43	3.24
PGA/PPE-CO_2-108 + HEPES + 300 mM NaCl	0.43	0.522	0.53	3.73
PGA/PPE-CO_2-108 + HEPES + 300 mM NaCl (Heated)	0.79	0.365	0.24	5.00

exhibited a lower absolute sensitivity of 0.0028 and 0.0038 $°C^{-1}$, respectively. When compared to other conjugated polymer-based thermal sensors, it also showed a significant advantage. For instance, the reported thermal sensor based on poly[5-methoxy-2-(3-sulfopropoxy)-1,4-phenylenevinylene] (MPS-PPV) prepared with poly(1-vinylpyrrolidone-*co*-styrene) (PVP-*co*-PS) had an absolute sensitivity of 0.015 $°C^{-1}$ between 20 and 90 °C.[24] The poly(3-hexylthiophene)-based sensor that was electrochemically doped

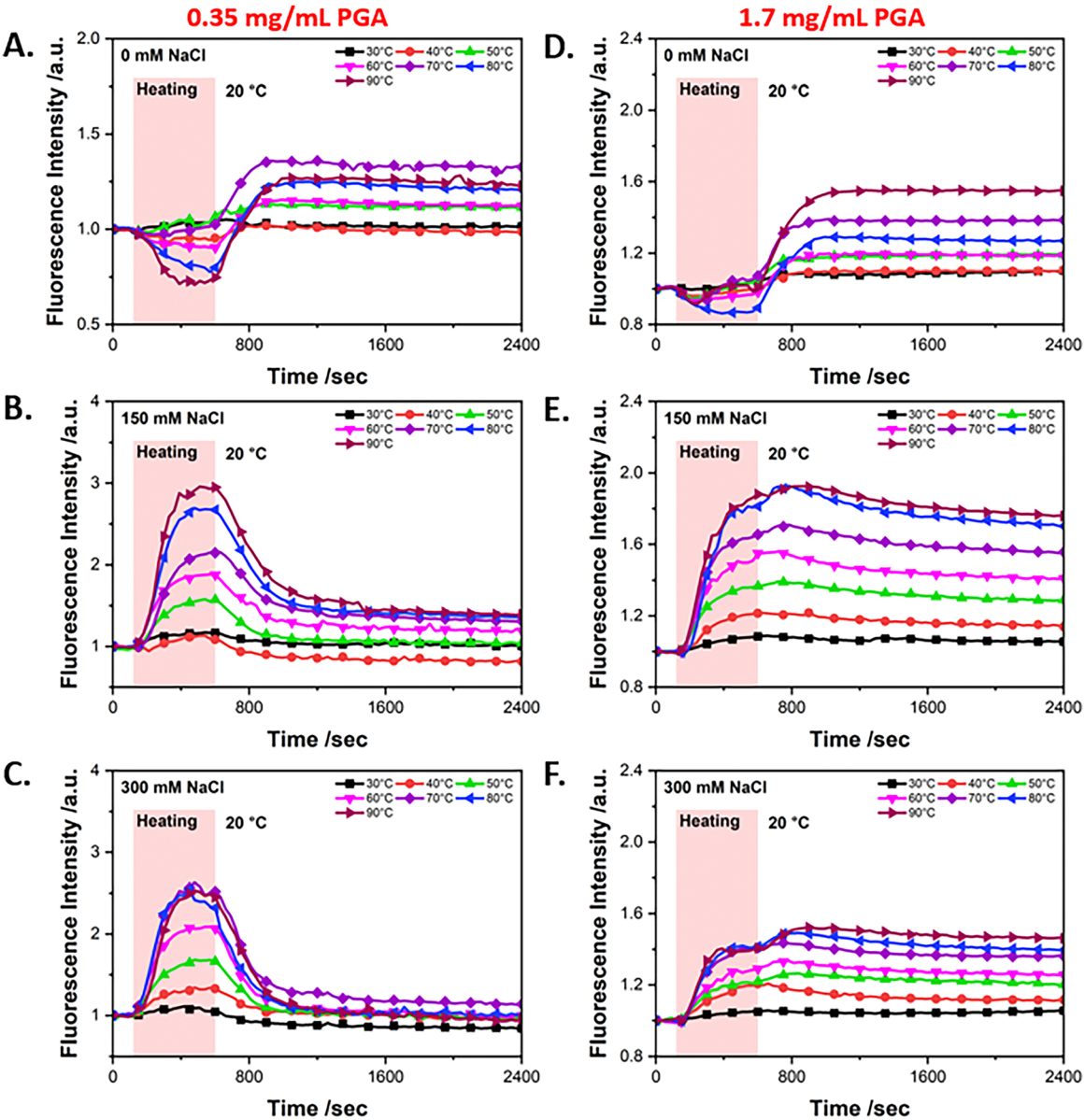

Fig. 4 Fluorescent temperature memory response of PPE-CO_2-108 with (A) 0.35 mg mL^{-1} PGA in HEPES buffer (10 mM, pH = 7.0) without NaCl, (B) with 150 mM NaCl and (C) 300 mM NaCl and with (D) 1.7 mg mL^{-1} PGA in HEPES buffer (10 mM, pH = 7.0) without NaCl, (E) with 150 mM NaCl and (F) 300 mM NaCl. The fluorescent time trajectories were measured at 450 nm after excitation at 405 nm. The samples were kept at 20 °C for 2 minutes. At t = 2 minutes, the temperature was increased, and the samples were kept at the desired temperature for 8 minutes before cooling back to 20 °C. Symbols are just for visual aid.

into thin films was reported to have an absolute sensitivity of 0.023 °C^{-1} measured between 30 and 75 °C.[45]

All these results confirmed our hypothesis that when the PGA/PPE-CO_2-108 solution is heated, PPE-CO_2 favors the disaggregated conformation. These free-conjugated polyelectrolytes are subsequently stabilized by the PGA macromolecules. To confirm these observations further, we measured the lifetime of the PGA/PPE-CO_2-108 complex at the lowest and highest NaCl concentrations (0 mM and 300 mM) at 20 °C and when heated to 90 °C (Table 1 and Fig. S3, ESI†). For non-heated samples, in the presence and absence of NaCl, the fluorescent lifetime consisted of a short and a slightly dominant long lifetime. When the solutions were heated and then measured, the presence of NaCl shifted the dominance toward the shorter lifetimes while at the low ionic strength solution, no major difference was observed. Non-aggregated conjugated polyelectrolytes have a predominately shorter lifetime. Previously, we have reported that upon the addition of PDDA, which stabilizes the individual polymer chains, the lifetime of PPE-CO_2-108 was predominantly at around 0.65 ns and the longer component contribution decreased with the increase in PDDA concentration.[25] The lifetime measurements confirm our hypothesis that in the absence of NaCl, a fraction of PPE-CO_2-108 chains are already destabilized, and the absorbed thermal energy goes to further disaggregate them before further stabilization by PGA.

Fluorescence signal memory effects in PGA/PPE-CO_2-108

Now that we have achieved our first goal in preparing a sensitive thermal sensor based on PGA macromolecules, we aimed to explore ways to test its reversibility. We have established so far that PPE-CO_2 thermal response alone is reversible, that the initial aggregated state played an important role in the thermal response, and that the dis/aggregation of CPEs was controlled by the PGA concentration and the solution ionic strength. In what follows, we unravel how we can control the reversibility of the PGA/PPE-CO_2-108 to achieve a thermal memory response. Different solutions of PGA/PPE-CO_2-108 samples (0.35 mg mL^{-1} or 1.7 mg mL^{-1} PGA in 0, 150, and 300 mM NaCl) were heated (red shade) and kept at the desired temperature for 8 minutes then cooled back to 20 °C (white shade), and monitored for 30 minutes. The resulting normalized fluorescent intensity time trajectories are presented in Fig. 4.

In the absence of NaCl for both PGA concentrations, we observed a slight decrease in the fluorescent intensity in the heating phase, followed by a rapid increase after cooling the solution to 20 °C. In the absence of NaCl, as we have established, the PPE-CO_2-108 is slightly disaggregated to start with. As such, the increase in the non-radiative pathway with temperature potentially overcomes any potential enhancement coming from further disaggregation. When the solution is cooled down, the non-radiative pathway diminishes resulting in an overall signal enhancement. The fact that this increase is more pronounced at lower PGA concentrations (lower number of stabilized CPEs) validates this hypothesis. In addition, the abrupt change in temperature, for instance, from 20 to 90 °C, could also limit the level of interaction between the two polymers resulting in less overall enhancement (Fig. S4, ESI†). In the presence of NaCl, the signal showed an increase in intensity. When the solution was cooled to 20 °C, only a limited number of experimental conditions exhibited a memory response, with the most significant result observed at 150 mM NaCl in the presence of 1.7 mg mL^{-1} PGA. We speculated that under this condition, the solution has enough PGA macromolecules to lock the PPE-CO_2-108 in the disaggregated more emissive state. Similar behavior was observed in a previous study from our laboratory when PPE-CO_2 was complexed with high molecular weight polyvinylpyrrolidone (PVP).[46]

To assess the long-term temperature memory of PGA/PPE-CO_2-108, we measured the thermal response profile of a solution prepared with 0.35 mg mL^{-1} PGA in HEPES (10 mM, pH = 7.0) without NaCl, 9 hours after being exposed to heating. While the presence of NaCl resulted in the highest short-term memory enhancement (Fig. 4E), as indicated by the overall measured improvement, its absence offered greater stability over the long term. After performing a heating cycle, the sample was cooled back to 20 °C and kept constant for up to 9 hours (Fig. 5). The intensity increased to 1.31 and remained stable at around 1.310 ± 0.008 from the initial recorded intensity. These memory measurements were crucial for clinical monitoring to capture skin temperature spikes even when they occur between measurement intervals.

As we conclude this section, we have shown that the thermal sensitivity, and most importantly the signal irreversibility, could be tuned by changing the PGA and the Na^+ concentrations. Next, we would study the performance of the PGA/PPE-CO_2-108 as dried films, which would mimic the state of sutures.

Fluorescence-based thermal sensing in PGA/PPE-CO_2-108 films

As stated before, our initial interest was to develop a thermal sensor able to detect infection by reporting temperature

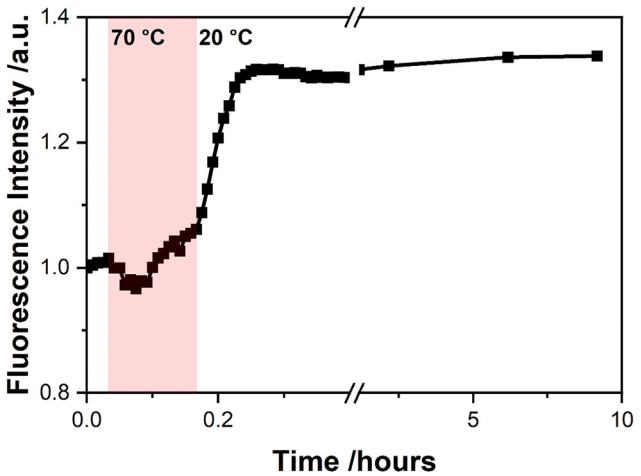

Fig. 5 Long-term fluorescent intensity time trajectory of PGA/PPE-CO_2-108 (up to 9 hours). The time trajectories were measured at 450 nm after excitation at 405 nm. The sample was kept at 20 °C for 2 minutes. At t = 2 minutes, the temperature was increased to 70 °C and kept for 8 minutes at this temperature before cooling it back to 20 °C. The fluorescent intensity was then measured at different time intervals. The sample was left in the dark between measurements.

changes on the wound site. As such, we studied the thermal sensing of PGA/PPE-CO_2-108 when prepared as dried films. Going from solution to thin polymeric films is often associated with changes in the microenvironment, conformational state, and potential changes in the interactions between the two polymers.[47]

PGA/PPE-CO_2-108 films were prepared in HEPES buffer with 300 mM NaCl before being dried into small thin polymeric film dots on a quartz slide and then placed on a temperature-controlled stage. Scanning electron microscopy images of the prepared films revealed a uniform texture at the macroscale, with minor roughness at the microscale level with a measured thickness of 3.4 mm (Fig. S5, ESI†). Unlike the thermal sensitivities obtained in solution, when the PGA/PPE-CO_2-108 was dried into films, the ones prepared from the highest ionic strength showed a slightly higher sensitivity (Fig. S6, ESI†). The temperature of the film was increased from room temperature to 90 °C, with 5 °C increments. The enhancement in fluorescent intensity could be observed by the change in the color intensity of the polymeric dots even to the naked eye. After each increase in temperature, the films were imaged by a DSLR Canon 750D camera equipped with a 60 mm macro lens under UV light. The images were further analyzed using ImageJ and the intensity of the red, green, and blue channels were extracted and plotted against the temperature change. The change in intensity of the green channel was more significant compared to the change of

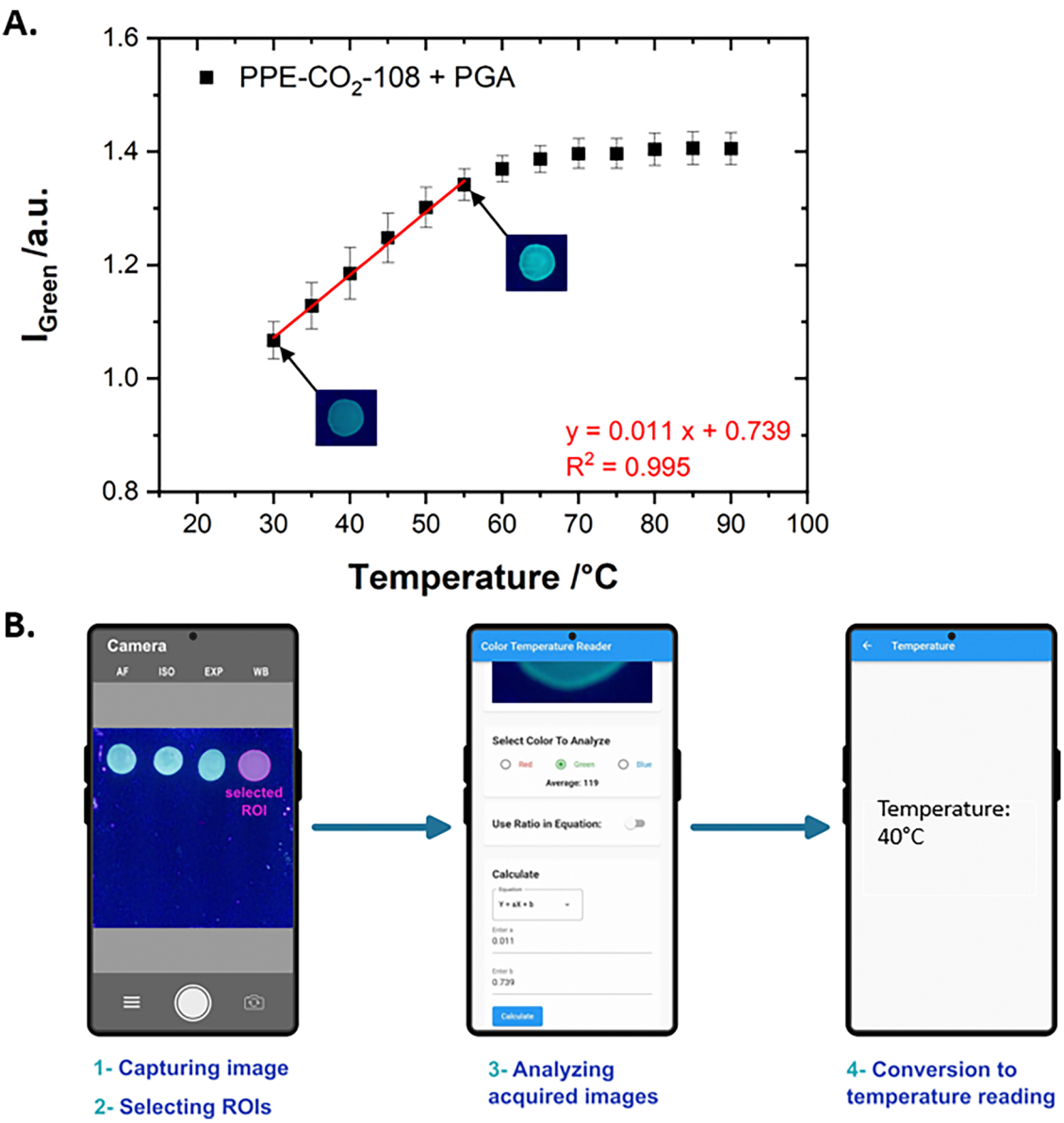

Fig. 6 (A) Fluorescent intensity changes obtained by dissecting the acquired images into their RGB components and plotting the average green intensity *versus* temperature. The images were acquired using a DSLR camera upon exiting a thin film of using a UV lamp between 30 °C and 90 °C. The thin film was prepared in HEPES buffer (10 mM, pH = 7.0; 300 mM NaCl). (B) Flow diagram showing how the PPE-CO_2-108/PGA films are imaged and converted into a temperature reading using the home-built smartphone application.

that of the blue channel (Fig. S7, ESI†) and it showed a linear increase till 55 °C with an absolute sensitivity of 0.011 $°C^{-1}$ (Fig. 6A) and maximum relative sensitivity of 1.3% $°C^{-1}$ at 25 °C and a temperature resolution of 2.0 °C. The films showed good photostability. Even after continuous UV irradiation for 1 hour, the fluorescence signal of the films decreased by only about 5% (Fig. S8, ESI†).

After demonstrating the thermal sensitivity of PGA/PPE-CO_2-108 films over a physiologically relevant temperature window, we developed an app to translate these changes in fluorescent signals to temperature readings. The app is able to extract the RGB colors and use the calibration curve obtained in Fig. 6A to calculate the film temperature. As a proof of concept, the films were heated to 40.0 °C, and images were taken using a smartphone and analyzed using the in-house developed app. The reported temperature of the films was 39.9 °C which showcases both the accuracy and practicality of the thermal sensor that we have developed (Fig. 6B). It also demonstrates its capability to be further developed and used in wound care applications. In a real-life setup, a wound temperature of 40 °C most likely indicates an infection.

Conclusion

In this work, we reported on the development of a thermal sensor prepared by complexing PGA with PPE-CO_2-108. The sensor was studied under different experimental conditions and its sensitivity and reversibility were therefore tuned. It successfully detected a wide range of temperatures, between 20 and 90 °C, with high absolute sensitivity. The tunable sensor can also act as a temperature memory reporter owing it to the irreversible disaggregation of PPE-CO_2-108 after a heating/cooling cycle at high PGA concentrations in the absence of NaCl. We also showed that the complex material is stable with long-lasting temperature memory which makes it a good candidate for applications over a long period of time. When prepared in a dry state, the sensor also displayed good thermal sensitivity between 20 and 55 °C which makes it physiologically relevant to monitor wound infections once prepared into strings for suture applications. While this study presents a promising step towards integrating thermal sensors into wound sutures for monitoring applications, several steps remain necessary to achieve this goal. The polymer complex needs to be properly formulated and tested to protect it from external factors such as humidity, changes in pH, and more to better reflect simulated wound bed conditions. In addition, an addon optoelectronic device needs to be developed to standardize the image capture parameters.

Materials

Poly(phenylene ethynylene) carboxylate (PPE-CO_2) with an average of 108 monomer repeating units was prepared using Sonagashira coupling following previously reported procedures.[29,48] Polygalacturonic acid (>90% enzymatic-50 g) was purchased from Sigma Aldrich. Sodium chloride, sodium hydroxide, and 4-(2-hydroxyethyl)-1-piperazineethanesulfonic acid (HEPES) were purchased from Fisher. Deionized water (18.2 MΩ cm) was used in all experiments.

Methods

Spectroscopic measurements. All steady-state fluorescence measurements were carried out using a Horiba Fluorolog-3 fluorometer equipped with a T3 Quantum Northwest temperature controller unit. The emission was measured between 435 nm and 650 nm after excitation at 405 nm. The integration time was set at 0.2 seconds. Standard 4 mL quartz cuvettes were used in all measurements with a total solution volume of 2 mL. Cuvettes were covered with Teflon caps to limit the solution evaporation at high temperatures. PGA stock solution was prepared by adding a few drops of sodium hydroxide to dissolve the polymer. PGA/PPE-CO_2-108 solution was prepared and left to stabilize for a few minutes at 20 °C in the sample holder, before taking any measurements. The mixture was constantly stirred at 400 RPM, to achieve temperature homogeneity. The temperature was typically increased by 5 °C at a time unless otherwise stated, and the spectra were measured 2 minutes after each temperature setting, allowing the mixture to homogenize. The fluorescent emission spectra of the time trajectories were measured at 450 nm, after excitation at 405 nm. In a typical fluorescence timescan, the sample was placed in the sample holder, at a temperature of 20 °C, and left for 10 minutes to stabilize. When the timescan started (t = 0 min), the sample was kept at 20 °C for 2 minutes, before increasing the temperature and holding it for 8 minutes. The temperature was then decreased back to 20 °C. The intensity of the fluorescent emission was measured every 30 seconds for a total of 40 minutes (unless otherwise specified). Absorbance measurements were recorded using PerkinElmer LAMBDA 1050+ UV/Vis/NIR spectrophotometer between 350 and 500 nm at room temperature.

Thermal imaging of dried PGA/PPE-CO_2-108. PGA/PPE-CO_2-108 was prepared in 50 μL of HEPES buffer (10 mM, pH = 7.0; 300 mM NaCl). The solution was vortexed and left for 30 minutes to stabilize. The mixture was then prepared into small polymeric dots on a glass slide and left for at least 4 hours in a dark place. The slide was then placed on a temperature-controlled stage (Linkam LTS 120) and the temperature was increased to 90 °C with 5 °C increments. At each temperature, the film was imaged, under UV light, using DSLR Canon 750D Camera. The intensities of the red, green, and blue color components were then analyzed using ImageJ.

Fluorescence lifetime measurements. A home-built confocal fluorescence microscopy setup (Olympus IX71) equipped with a high-numerical-aperture objective APON 60× (NA = 1.49) was used for the fluorescence lifetime measurements. The PGA/PPE-CO_2-108 samples prepared under different experimental conditions were excited at 405 nm using a fiber-coupled diode laser (PicoQuant GmbH, LDH-C-405) in quasi-continuous wave mode (pulsed excitation, 80 MHz repetition rate). The excitation light source was cleaned using an HC Laser Clean-up 405/10 filter (AHF analysentechnik AG) and was circularly polarized using a λ/4 waveplate. The fluorescence emission was collected

by focusing the laser beam inside the PGA/PPE-CO_2-108 solution which was reflected by a a dichroic mirror (AHF analysentechnik AG, 405RDC) and passed through a 405 nm long-pass filter (AHF analysentechnik AG) to remove any residual excitation light. The fluorescence signal was then recorded by a single-photon avalanche photodiode (Micro Photon Devices S.r.l., PDM series). The signal was recorded by a time-correlated single-photon counting (TCSPC) module (PicoQuant GmbH, HydraHarp 400) for extracting the lifetime measurements. Heated measurments came from the polymer mixture solutions that were heated first, cooled down and then measured on the microscope.

Data availability

The data supporting the findings of this study will be made available upon reasonable request. Interested researchers are encouraged to contact the corresponding author to arrange access within a mutually agreed timeframe.

Conflicts of interest

There are no conflicts to declare.

Acknowledgements

This work was supported by the University Research Board (#104391). The authors are also thankful to the Kamal A. Shair Central Research Science Lab (KAS CRSL) of the Faculty of Arts and Sciences at AUB for providing access to their facilities. P. K. is grateful to the Arab Fund Fellowships Program for their support, to the support of the Trilateral Research Group Linkages from the Humboldt Foundation, and to the research group of Prof. John Lupton and Dr Jan Vogelsang from the University of Regensburg for providing access to their facilities.

References

1 P. Bowler, B. Duerden and D. G. Armstrong, Wound microbiology and associated approaches to wound management, *Clin. Microbiol. Rev.*, 2001, **14**(2), 244–269.
2 G. Rath, T. Hussain, G. Chauhan, T. Garg and A. K. Goyal, Collagen nanofiber containing silver nanoparticles for improved wound-healing applications, *J. Drug Targeting*, 2016, **24**(6), 520–529.
3 M. C. Robson, Wound infection: a failure of wound healing caused by an imbalance of bacteria, *Surg. Clin. North Am.*, 1997, **77**(3), 637–650.
4 A. J. Singer and R. A. Clark, Cutaneous wound healing, *N. Engl. J. Med.*, 1999, **341**(10), 738–746.
5 P. Mistry, S. Kumar, R. S. Schloss, F. Berthiaume and N. A. Langrana, Chitosan-polygalacturonic acid complex dressing improves diabetic wound healing and hair growth in diabetic mice, *Biochem. Biophys. Res. Commun.*, 2024, **696**, 149502.
6 M. E. Zambroni, S. R. Martínez, G. E. Cagnetta, L. E. Ibarra, A. Posadaz, J. F. Martucci, S. Romanini, E. A. Aramayo, A. L. Cabral and P. Bertone, Multifunctional skin dressings synthesized via one-pot photopolymerization: Advancing wound healing and infection prevention strategies, *Polym. Adv. Technol.*, 2024, **35**(7), e6490.
7 R. Yadav, R. Kumar, M. Kathpalia, B. Ahmed, K. Dua, M. Gulati, S. Singh, P. J. Singh, S. Kumar, R. M. Shah, P. K. Deol and I. P. Kaur, Innovative approaches to wound healing: insights into interactive dressings and future directions, *J. Mater. Chem. B*, 2024, **12**(33), 7977–8006.
8 M. Abdollahi, A. Baharian, M. Mohamadhoseini, M. Hassanpour, P. Makvandi, M. Habibizadeh, B. Jafari, R. Nouri, Z. Mohamadnia and N. Nikfarjam, Advances in ionic liquid-based antimicrobial wound healing platforms, *J. Mater. Chem. B*, 2024, **12**(38), 9478–9507.
9 S. a Guo and L. A. DiPietro, Factors affecting wound healing, *J. Dent. Res.*, 2010, **89**(3), 219–229.
10 W. A. Sarhan, H. M. Azzazy and I. M. El-Sherbiny, Honey/chitosan nanofiber wound dressing enriched with Allium sativum and Cleome droserifolia: enhanced antimicrobial and wound healing activity, *ACS Appl. Mater. Interfaces*, 2016, **8**(10), 6379–6390.
11 P. Sim, X. L. Strudwick, Y. Song, A. J. Cowin and S. Garg, Influence of Acidic pH on Wound Healing In Vivo: A Novel Perspective for Wound Treatment, *Int. J. Mol. Sci.*, 2022, **23**, 21.
12 L. Bennison, C. Miller, R. Summers, A. Minnis, G. Sussman and W. McGuiness, The pH of wounds during healing and infection: a descriptive literature review, *Wound Pract. Res.*, 2017, **25**(2), 63–69.
13 S. Charkhabi, K. J. Jackson, A. M. Beierle, A. R. Carr, E. M. Zellner and N. F. Reuel, Monitoring Wound Health through Bandages with Passive LC Resonant Sensors, *ACS Sens.*, 2021, **6**(1), 111–122.
14 D. Arcangeli, I. Gualandi, F. Mariani, M. Tessarolo, F. Ceccardi, F. Decataldo, F. Melandri, D. Tonelli, B. Fraboni and E. Scavetta, Smart Bandaid Integrated with Fully Textile OECT for Uric Acid Real-Time Monitoring in Wound Exudate, *ACS Sens.*, 2023, **8**(4), 1593–1608.
15 F. Hu, Q. Gao, J. Liu, W. Chen, C. Zheng, Q. Bai, N. Sun, W. Zhang, Y. Zhang and T. Lu, Smart microneedle patches for wound healing and management, *J. Mater. Chem. B*, 2023, **11**(13), 2830–2851.
16 N. Pan, J. Qin, P. Feng, Z. Li and B. Song, Color-changing smart fibrous materials for naked eye real-time monitoring of wound pH, *J. Mater. Chem. B*, 2019, **7**(16), 2626–2633.
17 L. Wu, Y. He, H. Mao and Z. Gu, Bioactive hydrogels based on polysaccharides and peptides for soft tissue wound management, *J. Mater. Chem. B*, 2022, **10**(37), 7148–7160.
18 J. Jiang, J. Ding, X. Wu, M. Zeng, Y. Tian, K. Wu, D. Wei, J. Sun, Z. Guo and H. Fan, Flexible and temperature-responsive hydrogel dressing for real-time and remote wound healing monitoring, *J. Mater. Chem. B*, 2023, **11**(22), 4934–4945.
19 A. Chanmugam, D. Langemo, K. Thomason, J. Haan, E. A. Altenburger, A. Tippett, L. Henderson and T. A. Zortman, Relative temperature maximum in wound

infection and inflammation as compared with a control subject using long-wave infrared thermography, *Adv. Skin Wound Care*, 2017, **30**(9), 406–414.
20 M. S. Brown, K. Browne, N. Kirchner and A. Koh, Adhesive-Free, Stretchable, and Permeable Multiplex Wound Care Platform, *ACS Sens.*, 2022, **7**(7), 1996–2005.
21 G. H. Darwish, A. Koubeissi, T. Shoker, S. A. Shaheen and P. Karam, Turning the heat on conjugated polyelectrolytes: an off–on ratiometric nanothermometer, *Chem. Commun.*, 2016, **52**(4), 823–826.
22 G. H. Darwish, H. H. Fakih and P. Karam, Temperature Mapping in Hydrogel Matrices Using Unmodified Digital Camera, *J. Phys. Chem. B*, 2017, **121**(5), 1033–1040.
23 S. R. Yassine, S. A. Hassoun and P. Karam, Fluorescent thermal sensing using conjugated polyelectrolytes in thin polymer films, *Anal. Chim. Acta*, 2019, **1077**, 249–254.
24 K. Alhafi, N. Merhi and P. Karam, Single Particle Insights into the Thermal Sensing of Conjugated Polyelectrolyte–Nanoparticle Assemblies, *ACS Appl. Opt. Mater.*, 2024, **2**(10), 2118–2127.
25 J. Kaj and P. Karam, Self-Referenced Temperature Sensor Based on Conjugated Polyelectrolytes, *ACS Appl. Polym. Mater.*, 2024, **6**(12), 7036–7046.
26 S. Hassoun and P. Karam, Fluorescent-Based Thermal Sensing in Lipid Membranes, *Langmuir*, 2020, **36**(5), 1221–1226.
27 G. H. Darwish, J. Abouzeid and P. Karam, Tunable nanothermometer based on short poly(phenylene ethynylene), *RSC Adv.*, 2016, **6**(71), 67002–67010.
28 P. Karam, A. A. Hariri, C. F. Calver, X. Zhao, K. S. Schanze and G. Cosa, Interaction of Anionic Phenylene Ethynylene Polymers with Lipids: From Membrane Embedding to Liposome Fusion, *Langmuir*, 2014, **30**(35), 10704–10711.
29 X. Zhao, H. Jiang and K. S. Schanze, Polymer Chain Length Dependence of Amplified Fluorescence Quenching in Conjugated Polyelectrolytes, *Macromolecules*, 2008, **41**(10), 3422–3428.
30 M.-W. Lee, C.-L. Hung, J.-C. Cheng and Y.-J. Wang, A new anti-adhesion film synthesized from polygalacturonic acid with 1-ethyl-3-(3-dimethylaminopropyl) carbodiimide cross-linker, *Biomaterials*, 2005, **26**(18), 3793–3799.
31 J. Schmidgall and A. Hensel, Bioadhesive properties of polygalacturonides against colonic epithelial membranes, *Int. J. Biol. Macromol.*, 2002, **30**(5), 217–225.
32 A. T. Ngo, P. Karam and G. Cosa, Conjugated polyelectrolyte–lipid interactions: Opportunities in biosensing, *Pure Appl. Chem.*, 2010, **83**(1), 43–55.
33 L. P. Fernando, P. K. Kandel, J. Yu, J. McNeill, P. C. Ackroyd and K. A. Christensen, Mechanism of cellular uptake of highly fluorescent conjugated polymer nanoparticles, *Biomacromolecules*, 2010, **11**(10), 2675–2682.
34 J. H. Moon, W. McDaniel, P. MacLean and L. F. Hancock, Live-cell-permeable poly (p-phenylene ethynylene), *Angew. Chem., Int. Ed.*, 2007, **46**(43), 8223.
35 T. Abou Matar and P. Karam, The Role of Hydrophobicity in the Cellular Uptake of Negatively Charged Macromolecules, *Macromol. Biosci.*, 2018, **18**(2), 1700309.
36 M. Wu, P. Kaur, H. Yue, A. Clemmens, D. H. Waldeck, C. Xue and H. Liu, Charge density effects on the aggregation properties of poly (p-phenylene-ethynylene)-based anionic polyelectrolytes, *J. Phys. Chem. B*, 2008, **112**(11), 3300–3310.
37 Y. Hattori, N. Nishimura, Y. Tsutsui, S. Ghosh, T. Sakurai, K. Sugiyasu, M. Takeuchi and S. Seki, Rod-like transition first or chain aggregation first? ordered aggregation of rod-like poly (p-phenyleneethynylene) chains in solution, *Chem. Commun.*, 2019, **55**(89), 13342–13345.
38 M. Mahmoud, A. Poncheri and M. El-Sayed, Properties of π-conjugated fluorescence polymer–plasmonic nanoparticles hybrid materials, *J. Phys. Chem. C*, 2012, **116**(24), 13336–13342.
39 J. Kaj and P. Karam, Self-Referenced Temperature Sensor Based on Conjugated Polyelectrolytes, *ACS Appl. Polym. Mater.*, 2024, **6**(12), 7036–7046.
40 G. H. Darwish and P. Karam, Nanohybrid conjugated polyelectrolytes: highly photostable and ultrabright nanoparticles, *Nanoscale*, 2015, **7**(37), 15149.
41 H. Jiang, X. Zhao and K. S. Schanze, Amplified fluorescence quenching of a conjugated polyelectrolyte mediated by Ca^{2+}, *Langmuir*, 2006, **22**(13), 5541–5543.
42 G. H. Darwish, A. Koubeissi, T. Shoker, S. Abou Shaheen and P. Karam, Turning the heat on conjugated polyelectrolytes: an off–on ratiometric nanothermometer, *Chem. Commun.*, 2016, **52**(4), 823–826.
43 G. H. Darwish, J. Abouzeid and P. Karam, Tunable nanothermometer based on short poly (phenylene ethynylene), *RSC Adv.*, 2016, **6**(71), 67002–67010.
44 S. H. Lee, S. Kömürlü, X. Zhao, H. Jiang, G. Moriena, V. D. Kleiman and K. S. Schanze, Water-Soluble Conjugated Polyelectrolytes with Branched Polyionic Side Chains, *Macromolecules*, 2011, **44**(12), 4742–4751.
45 H. Maddali, A. M. Tyryshkin and D. M. O'Carroll, Dual-mode polymer-based temperature sensor by dedoping of electrochemically doped, conjugated polymer thin films, *ACS Appl. Electron. Mater.*, 2021, **3**(11), 4718–4725.
46 J. Kaj, D. Hussein and P. Karam, Fluorescent-Based Temperature Memory Reporter for Nanoscale Thermal Measurements, *J. Phys. Chem. C*, 2022, **126**(48), 20542–20549.
47 I. A. Levitsky, J. Kim and T. M. Swager, Energy Migration in a Poly (phenylene ethynylene): Determination of Interpolymer Transport in Anisotropic Langmuir– Blodgett Films, *J. Am. Chem. Soc.*, 1999, **121**(7), 1466–1472.
48 X. Zhao, *Conjugated polyelectrolytes based on poly (arylene ethynylene): Synthesis, solution photophysics and applications to sensors and solar cells*, 2007.